

An X-ray review of MS 1054-0321: hot or not? *

I. M. Gioia¹, V. Braito², M. Branchesi^{1,3}, R. Della Ceca², T. Maccacaro² and K.-V. Tran⁴

¹ Istituto di Radioastronomia del CNR-INAf, Via P. Gobetti 101, I-40129 Bologna, Italy
e-mail: gioia@ira.cnr.it

² INAF - Osservatorio Astronomico di Brera, Via Brera 28, I-20121 Milano, Italy
e-mail: braitto@brera.mi.astro.it, e-mail: rdc@brera.mi.astro.it, e-mail: tommaso@brera.mi.astro.it

³ Dipartimento Astronomia Università di Bologna, Via Ranzani 1, I-40127 Bologna, Italy
e-mail: mbranch@ira.cnr.it

⁴ Institute for Astronomy, ETH Hoenggerberg, HPF G4.2 CH-8093 Zurich, Switzerland
e-mail: vy@phys.ethz.ch

Received; accepted

Abstract. XMM-Newton observations are presented for the $z = 0.83$ cluster of galaxies MS 1054–0321, the highest redshift cluster in the *Einstein* Extended Medium Sensitivity Survey (EMSS). The temperature inferred by the XMM-Newton data, $T=7.2^{+0.7}_{-0.6}$ keV, is much lower than the temperature previously reported from ASCA data, $T=12.3^{+3.1}_{-2.2}$ keV (Donahue et al. 1998), and a little lower than the Chandra temperature, $T=10.4^{+1.7}_{-1.5}$ keV, determined by Jeltema et al. 2001. The discrepancy between the newly derived temperature and the previously derived temperatures is discussed in detail. If one allows the column density to be a free parameter, then the best fit temperature becomes $T=8.6^{+1.2}_{-1.1}$ keV, and the best fit column density becomes $N_H = 1.33^{+0.15}_{-0.14} \times 10^{20}$ atoms cm^{-2} . The iron line is well detected in the XMM-Newton spectrum with a value for the abundance of $Z=0.33^{+0.19}_{-0.18} Z_\odot$, in very good agreement with previous determinations. The derived XMM X-ray luminosity for the overall cluster in the 2–10 keV energy band is $L_X = (3.81 \pm 0.19) \times 10^{44} \text{ h}^{-2} \text{ erg s}^{-1}$ while the bolometric luminosity is $L_{\text{BOL}} = (8.05 \pm 0.40) \times 10^{44} \text{ h}^{-2} \text{ erg s}^{-1}$. The XMM-Newton data confirm the substructure in the cluster X-ray morphology already seen by ROSAT and in much more detail by Chandra. We find that only two of the three clumps detected in the weak lensing mass reconstruction image are visible in X-rays, as already noted by Jeltema et al. (2001). The central weak lensing clump is coincident with the main cluster component and has a temperature $T=8.1^{+1.3}_{-1.2}$ keV. The western weak lensing clump coincides with the western X-ray component which is much cooler with a temperature $T=5.6^{+0.8}_{-0.6}$ keV. The optically measured velocity dispersion, obtained from 145 cluster redshifts, is consistent with the velocity dispersion expected from the $\sigma_V - T_X$ relationship once the XMM-Newton temperature is used. MS 1054–0321 fits well in the $\sigma \propto T^{1/2}$ correlation available in the literature and derived from information collected for all clusters at redshifts of $z \leq 1.27$ known today and with a measured X-ray temperature. The cluster temperature seems to be commensurate with the predictions from its X-ray luminosity from the $L_X - T_X$ relation of local clusters. Given the newly determined temperature, MS 1054–0321 is no longer amongst the hottest clusters known.

Key words. galaxies: clusters: general, dark matter, intergalactic medium, cosmology, individual, MS 1054-0321 – X-rays: observations: general

1. Introduction

MS 1054–0321 is the most luminous and distant cluster of galaxies in the EMSS (Gioia et al. 1990; Stocke et al. 1991). For some time it was the only very massive, high redshift cluster of galaxies (Gioia & Luppino 1994), hence it was extensively studied and observed at many different wavelengths. Donahue et al. (1998) performed an X-ray analysis using both ASCA and ROSAT and determined a high luminosity ($L_{\text{BOL}} = 1.1 \times 10^{45} h_{100}^{-2} \text{ erg s}^{-1}$) and high gas temperature ($T=12.3^{+3.1}_{-2.2}$ keV). Using this temperature Donahue et al. estimated a virial mass of $\sim 7.4 \times 10^{14} h_{100}^{-1} M_\odot$ within a radius $r_{500}^1 = 1.5 h_{100}^{-1} \text{ Mpc}$. The X-ray emission of MS 1054–0321 is resolved by the ROSAT/HRI in two,

Send offprint requests to: I. M. Gioia

* Data presented here used the XMM-Newton facility

¹ within a region whose density is 500 times the critical density.

Fig. 1. X-ray image of the MOS2 detector showing the extended emission of MS 1054–0321. This image is presented to highlight the four different regions analyzed in X-rays. Figure 1 can be seen in the pdf file of the paper at <http://www.ira.cnr.it/~gioia/PUB/publications.html>

possibly three clumps, plus an extended component indicating that the cluster is not relaxed and that some caution must be adopted when determining parameters from the X-ray data. Neumann & Arnaud (2000) used the same ASCA temperature and an isothermal β model fit to the ROSAT/HRI data to obtain a total mass of $1.6 \times 10^{15} h_{50}^{-1} M_{\odot}$ within a virial radius $r_V = 1.65 h_{50}^{-1}$ Mpc. The significant substructure observed in the HRI data by the above investigators was confirmed by Jeltema et al. 2001 (J01) who used the superb resolution of the Chandra instruments. J01 give a new determination of the temperature, $T=10.4_{-1.5}^{+1.7}$ keV, lower than the ASCA temperature and measured, consequently, a lower virial mass of $6.2 \times 10^{14} h_{100}^{-1} M_{\odot}$ within $r_{200}^2 = 0.76 h_{100}^{-1}$ Mpc. A similar temperature for MS 1054–0321 was found by Joy et al. (2001) using Sunyaev Zeldovich Effect data. They derive a temperature $T=10.4_{-2}^{+5}$ keV and a total mass within $94''$ (corresponding to 389 kpc in the cosmology adopted in this paper) equal to $M(\leq 94'') = (4.6 \pm 0.8) \times 10^{14} h_{100}^{-1} M_{\odot}$. Vikhlinin et al. (2002) used the Chandra instruments, and derived an even lower value for the temperature, $T=7.8 \pm 0.6$ keV, in agreement with the determination by Tozzi et al. (2003) who analyzed the same Chandra data and obtained $T=8.0 \pm 0.5$ keV. In the optical band an extensive study by Tran et al. (1999) and van Dokkum et al. (2000), based on 24 and 81 spectroscopic cluster member redshifts, respectively, finds agreement between the observed velocity dispersion ($\sigma_V = 1170 \pm 150$ km s $^{-1}$; Tran et al. 1999) and the high X-ray measured ASCA temperature ($T=12.3_{-2.2}^{+3.1}$ keV; Donahue et al. 1998), albeit within the large errors. From Hubble Space Telescope (HST) imaging, supplemented by ground telescope data, van Dokkum et al. (2000) detected a large overdensity of red cluster galaxies with irregular and elongated distribution. A very high fraction (17 per cent) of the cluster galaxies are classified as “mergers/peculiar” on the basis of double nuclei, tidal tails and distorted morphologies (see van Dokkum et al. 1999; van Dokkum et al. 2000).

Hoekstra, Franx & Kuijken (2000) performed a weak lensing study using a two-color mosaic of deep WFPC2 images and determined a mass of $(1.2 \pm 0.2) \times 10^{15} h_{50}^{-1} M_{\odot}$ within an aperture radius $1 h_{50}^{-1}$ Mpc, in good agreement with the previous estimators (Luppino & Kaiser 1997; Clowe et al. 2000). Assuming an isothermal mass distribution Hoekstra, Franx & Kuijken (2000) found a corresponding velocity dispersion of 1311_{-89}^{+83} km s $^{-1}$, again consistent with the X-ray and optical estimates. The weak lensing signal clearly shows three distinct clumps in the mass reconstruction distribution in agreement with the light distribution, that all appear to have similar masses.

An extremely deep 5-GHz survey of the cluster region down to 32 μ Jy (6σ ; Best et al. 2000) detects a high number of radio sources (34 vs 25 expected from blank-field radio source counts). Surprisingly, no radio emission is detected towards the merger galaxies found in the HST images by van Dokkum et al. (2000) consistent with the hypothesis that low-luminosity radio sources may be triggered by initial weak interactions rather than direct mergers (Best et al. 2000). Johnson, Best & Almaini (2003) detected an excess of point sources in the archival deep Chandra image of the field of MS 1054–0321. Combined with identifications of cluster AGN from the radio work of Best et al. (2002), MS 1054–0321 seems to have a significantly enhanced AGN activity with respect to local galaxy clusters.

From all these data a consistent picture emerges of MS 1054–0321 as a young, massive, highly luminous cluster with significant substructure both in the X-ray and optical data, confirmed by the weak lensing mass reconstruction distribution. MS 1054–0321 was also observed by XMM-Newton. The new data analysis and interpretation are the subject of this paper. A new redshift determination from additional optical spectroscopic data is used in combination with the XMM-Newton data to provide a more accurate picture of the cluster. Comparisons are also made with previous analyses. Throughout the paper we use a Hubble constant of $H_0 = 100h$ km s $^{-1}$ Mpc $^{-1}$, $q_0 = 0.5$ (for comparison with previous work on this cluster) and a cosmological constant of $\Lambda = 0$, except where noted. One arcmin corresponds to 248.6 h $^{-1}$ kpc at the cluster redshift.

2. XMM-Newton Data

2.1. Observations and Data Analysis

XMM-Newton observed MS 1054–0321 as part of the GTO program, on June 21, 2001 for about 40 Ks (Seq # 0094800101). The European Photon Imaging Camera (EPIC), which incorporates one pn and two MOS CCD arrays (Sröder 2001; Turner et al. 2001) was operating in full-frame mode with the thin filter applied. Unfortunately the observations suffer from time periods of very high background. Event files produced from the standard pipeline processing have been examined and filtered (using the version 5.4 of the Science Analysis Software, SAS, and the latest calibration files released by the EPIC team) to remove the high background time intervals. Only events corresponding

² within a region whose density is 200 times the critical density.

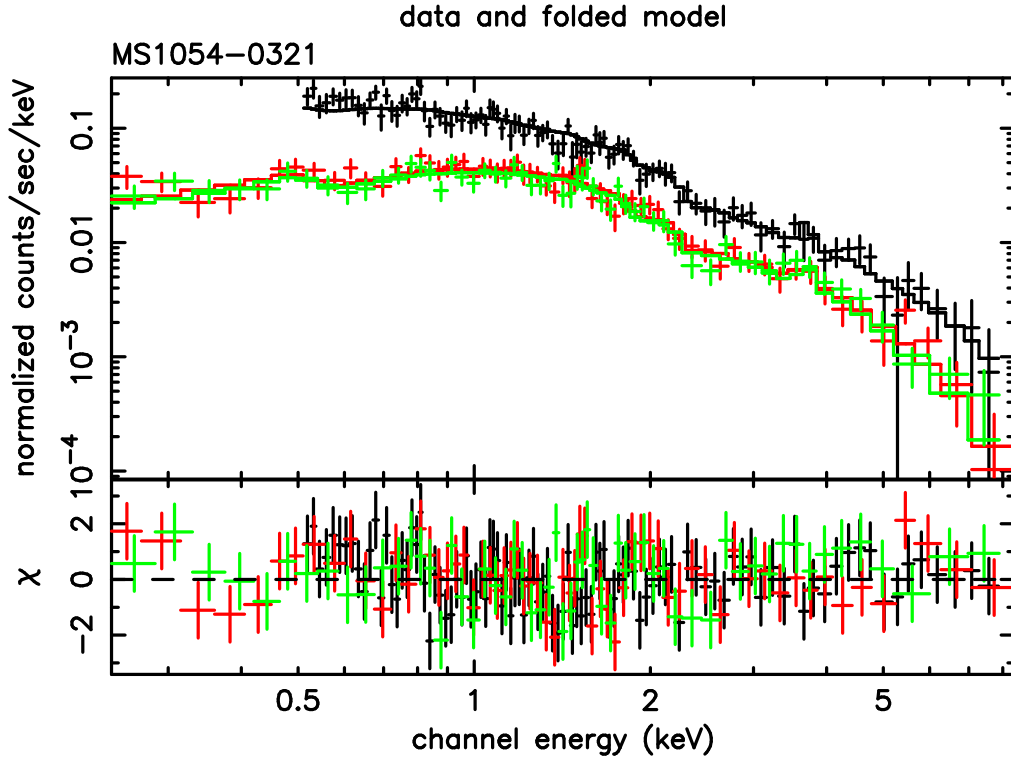


Fig. 2. Binned X-ray spectrum and residuals for MS 1054–0321. The spectrum was binned to have a minimum of 40 (50) counts per bin for each MOS (pn). The solid line represents the the best fit MEKAL model.

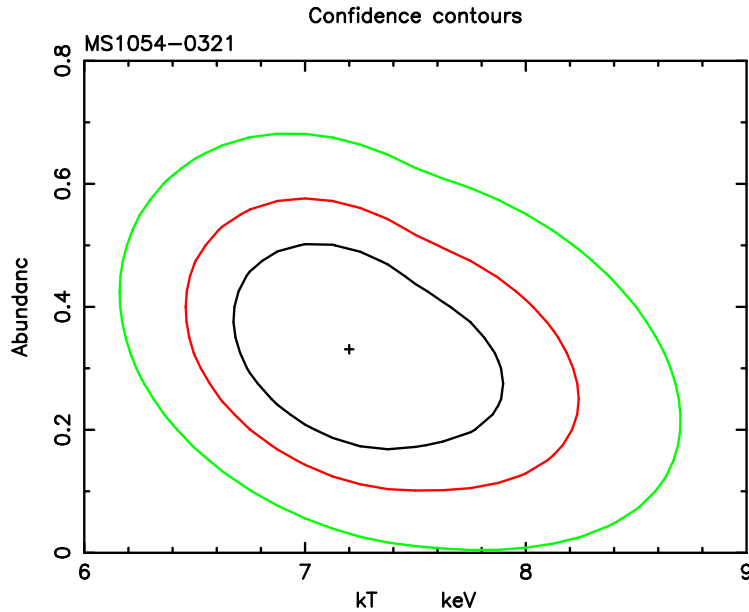


Fig. 3. 68.3%, 90%, and 99% confidence χ^2 contours ($\Delta\chi = 2.30, 4.61, \text{ and } 9.21$) for the cluster iron abundance and temperature (point source to the south excluded).

to pattern 0-12 for MOS and pattern 0-4 for pn have been used³. The net exposure times, after data cleaning, are ~ 28.4 Ks and ~ 29 Ks for MOS 1 and MOS 2, respectively, and ~ 21.9 Ks for pn. Background counts have been accumulated using nearby source-free circular regions. This observation suffers from high mean background level thus the use of a local background estimate is more appropriate than the blank-sky background which would lead to an underestimate of the background counts. Response matrices (that include the correction for the effective area) have

³ see the XMM-Newton Users' Handbook
http://xmm.vilspa.esa.es/external/xmm_user_support/documentation/uhb/XMM_UHB.htm

been generated using the SAS tasks *arfgen* and *rmfgen*. The X-ray fluxes reported below are computed using the MOS2 detector and calibration(s). The normalization of the MOS1 is about 2% higher than for MOS2 whereas the normalization of the pn is 7.5% higher.

2.2. Overall Cluster Properties

Fig. 1 shows the XMM-Newton MOS2 image of MS 1054–0321. The X-ray cluster is elongated in the east-west direction and follows the distribution of optical galaxies well visible in the I-band image of MS 1054–0321 shown in Fig. 7. The point source to the south is also marked. The X-ray image has two distinct components (Component 1 and Component 2) plus a fainter emission region (indicated as Component 3 in the figure) between the cluster main emission and the point source emission.

In order to measure the emission-weighted cluster temperature, net counts were extracted from a circle of radius 1.5' centered at $\alpha_{2000} = 10^h 56^m 58.7^s$, $\delta_{2000} = -03^\circ 37' 45''$ in the MOS1 and MOS2 detectors. The 1.5' radius was chosen to have the same parameters previously used by J01 in order to compare our results with theirs. There are 2392 ± 54 net counts, in the 0.2–8 keV energy range, in MOS2 (2198 ± 52 in MOS1) and 4486 ± 75 net counts in the pn detector (the pn counts are taken in the 0.5–8 keV band to avoid calibration uncertainties of the pn in the softer energy band). The data were fitted with a MEKAL model (Mewe, Gronenschild & van den Oord, 1985) modified by Galactic absorption. The absorption and redshift were kept constant while the abundance and temperature were left free to vary. The Galactic absorption was fixed at the Galactic value of 3.6×10^{20} atoms cm^{-2} (Dickey & Lockman 1990), and the redshift was fixed at $z=0.83$ (Tran et al. 1999; van Dokkum et al. 2000). The point source to the south (indicated as Point Source in Fig. 1) at $\alpha_{2000} = 10^h 56^m 58.8^s$, $\delta_{2000} = -03^\circ 38' 52''$, corresponds to the point source previously seen as an extension to the south in the ROSAT HRI data, and as a point source in the Chandra image published by J01. This source was excluded from the analysis of the cluster by masking a circular region with radius 15'', and will be discussed later. The best fit with a thermal MEKAL model gives a temperature $T=7.2^{+0.7}_{-0.6}$ keV and an abundance $Z=0.33^{+0.19}_{-0.18} Z_\odot$, relative to the abundances of Grevesse & Sauval (1998)⁴. The best fit X-ray spectral parameters are listed in Table 1. Throughout this paper quoted uncertainties are 90% confidence levels for one interesting parameter.

The binned X-ray spectrum and best fit folded model are shown in Fig. 2 where bins include at least 40 counts each (50 counts each for the pn). The fit has an acceptable reduced χ^2 of 0.986 for 219 degrees of freedom. The χ^2 contours for iron abundance versus cluster temperature are shown in Fig. 3. The absorbed flux in the 2–10 keV energy band, excluding the point-like source to the south, is $F_X = (3.40 \pm 0.17) \times 10^{-13}$ erg cm^{-2} s^{-1} . The unabsorbed K-corrected luminosity in the same energy band is $L_X = (3.81 \pm 0.19) \times 10^{44}$ h⁻² erg s^{-1} while the bolometric luminosity is $L_{\text{BOL}} = (8.05 \pm 0.40) \times 10^{44}$ h⁻² erg s^{-1} . Given the detection of the iron line, we can thaw the redshift parameter in XSPEC and fit for it. The best fit for the redshift is $z=0.847^{+0.057}_{-0.040}$, in very good agreement with the optical spectroscopic determination.

We have then fitted the data allowing the N_H to be a free parameter and using a one-temperature MEKAL model. The resulting value for the column density is $N_H = 1.33^{+0.15}_{-0.14} \times 10^{20}$ atoms cm^{-2} , lower than the Galactic value, and the resulting temperature is $T=8.6^{+1.2}_{-1.1}$ keV, higher than when freezing the N_H . The abundance becomes $Z=0.22^{+0.15}_{-0.14} Z_\odot$, and the reduced χ^2 is 0.923 for 218 degrees of freedom. This result goes in the same direction as the result by Tozzi et al. 2003 for MS 1054–0321 (see their Fig. 12) where they also obtain an higher temperature (~ 10 keV) and a lower column density value when they allow the N_H to vary.

We have also explored the effect of fitting a two-temperature MEKAL model to the data to check if there is a soft emission coming from a cooler temperature plasma, due to the presence of groups and poor clusters emission falling into the larger cluster. We obtain a value for the column density lower than the Galactic value: N_H goes from 1.3×10^{20} to 2.6×10^{20} atoms cm^{-2} , while the two temperatures assume values of ~ 0.2 keV and ~ 9 keV but with a great degeneracy which makes impossible to assign any error to the fit. From a purely statistical point of view, the addition of the softer thermal component is not supported by the F-test (Bevington & Robinson, 1992).

2.3. Cluster Substructure

Jeltema et al. (2001) show in Fig. 9 of their paper that the central and western clumps of the weak lensing study correspond to the eastern and western Chandra X-ray clumps, respectively. Several galaxies lie at the position of the eastern clump, including the cD, while the western clump appears to have galaxies which are lining the southern edge

⁴ As suggested by Gastaldello & Molendi (2002), we have adopted the Grevesse & Sauval values since the community has converged towards a “standard solar composition” given the discrepancies between meteoritic and photospheric solar abundances, particularly for iron, as quoted in a review by Anders & Grevesse (1989). We note that using the ratio between the elements fixed to the solar values of Grevesse & Sauval results in abundance values higher by a factor 1/0.676 than using the solar values of Anders & Grevesse (1989). This is due to the fact that Grevesse & Sauval use a 0.676 times lower iron abundance.

Fig. 4. X-ray spectrum and residuals for the eastern X-ray component (Component 1) within a $0.47'$ radius circle. The spectrum was binned to have a minimum of 20 counts per bin. The solid line represents the best fit MEKAL model. The insert shows the 68.3%, 90%, and 99% confidence χ^2 contours (corresponding to $\Delta\chi^2 = 2.30, 4.61,$ and 9.21) for the iron abundance and temperature. Figure 4 can be seen in the pdf file of the paper at <http://www.ira.cnr.it/~gioia/PUB/publications.html>

Fig. 5. X-ray spectrum and residuals for the western X-ray component (Component 2) within a $0.47'$ radius circle. The spectrum was binned to have a minimum of 20 counts per bin. The insert shows the 68.3%, 90%, and 99% confidence χ^2 contours (corresponding to $\Delta\chi^2 = 2.30, 4.61,$ and 9.21) for the iron abundance and temperature. Figure 5 can be seen in the pdf file of the paper at <http://www.ira.cnr.it/~gioia/PUB/publications.html>

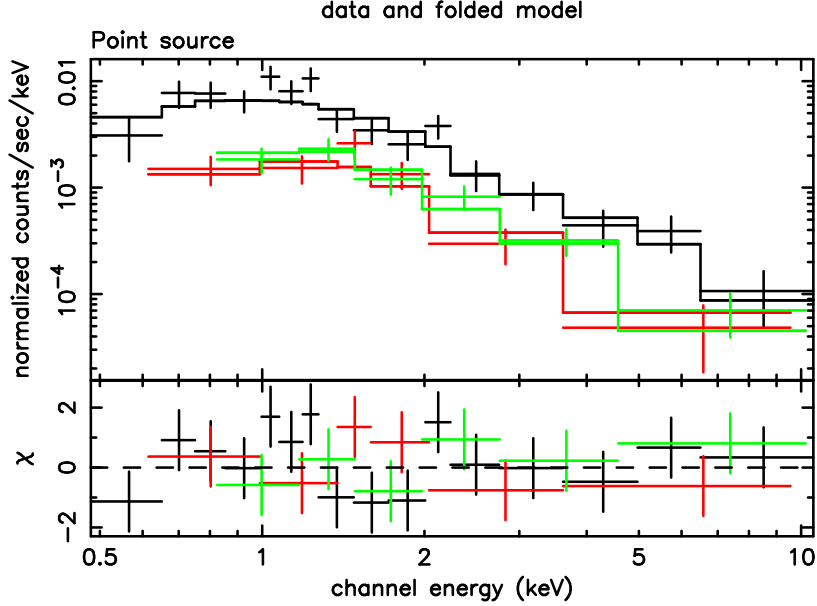


Fig. 6. X-ray spectrum and residuals for the point source to the south of the cluster within a $0.33'$ radius circle. The spectrum was binned to have a minimum of 20 counts per bin. The solid line represents the best fit power law model.

of the clump. We have enough statistics in the *XMM-Newton* data to examine the two X-ray peaks (Component 1 and Component 2) separately by putting an extraction circle of radius $0.47'$ centered on each peak. The $0.47'$ radius was chosen to avoid overlapping the extraction circles placed on the two separate clumps and thus any possible contamination between them (see Fig. 1). For the eastern component the center was fixed at $\alpha_{2000} = 10^h 57^m 00.3^s$, $\delta_{2000} = -03^\circ 37' 28.8''$, while the western peak is centered at $\alpha_{2000} = 10^h 56^m 56.6^s$, $\delta_{2000} = -03^\circ 37' 36.3''$. There are between 580 and 660 net counts in each clump according to which MOS is considered (see Table 1), and approximately over twice this number of counts in the pn. In total there are 2387 ± 49 net counts in the eastern clump and 2245 ± 50 net counts in the western clump. The spectrum of each clump was fitted with a MEKAL model with the N_H fixed at the Galactic value of 3.6×10^{20} atoms cm^{-2} , the redshift fixed at 0.83, and the iron abundance and temperature were left free to vary. Given the reduced statistics with respect to the cluster as a whole, the data were binned to include a minimum of 20 counts per bin. The eastern component has a best-fit temperature of $T = 8.1^{+1.3}_{-1.2}$ keV with a reduced χ^2 of 1.4 for 115 degrees of freedom. This temperature is consistent with the cluster temperature, while the western component is somewhat cooler with a best-fit temperature of $T = 5.6^{+0.8}_{-0.6}$ keV and a reduced χ^2 of 1.26 for 110 degrees of freedom. The spectra and best-fit models are shown in Fig. 4 and Fig. 5. The western clump was found to be cooler also in the Chandra analysis by J01 who quote a temperature $T = 10.5^{+3.4}_{-2.1}$ keV for the eastern clump, and $T = 6.7^{+1.7}_{-1.2}$ keV for the western clump. We find the iron abundances of the eastern and western components to be $Z = 0.12^{+0.35}_{-0.12} Z_\odot$ and $Z = 0.51^{+0.36}_{-0.32} Z_\odot$, respectively. Given the large uncertainties these abundances are found to be consistent between each other and with the cluster abundance. Similar results were found by J01 even if their abundances are relative to Anders & Grevesse (1989). The absorbed fluxes in 2–10 keV for the two clumps are $F_{X,east} = (9.69 \pm 0.67) \times 10^{-14}$ erg $\text{cm}^{-2} \text{s}^{-1}$ and $F_{X,west} = (6.94 \pm 0.59) \times 10^{-14}$ erg $\text{cm}^{-2} \text{s}^{-1}$, respectively, while the unabsorbed K-corrected luminosities in the same energy bands are $L_{X,east} = (1.05 \pm 0.07) \times 10^{44}$ erg s^{-1} and $L_{X,west} = (8.69 \pm 0.73) \times 10^{43}$ erg s^{-1} . The respective bolometric luminosities are $L_{BOL,east} = (2.23 \pm 0.15) \times 10^{44}$ erg s^{-1} and $L_{BOL,west} = (1.82 \pm 0.15) \times 10^{44}$ erg

s^{-1} . We attempted to examine also the emission region marked as Component 3 in Fig. 1 by putting an extraction circle of radius $0.47'$ centered as indicated in the figure. A higher temperature than the cluster as a whole is found of $T=8.2_{-1.71}^{+2.45}$ keV, and an abundance of $Z=0.23_{-0.23}^{+0.63} Z_{\odot}$. The large errors are due to the reduced statistics. There are only ~ 350 net counts per detector. Given the small number of photons, this emission region will not be considered any further.

As previously noted by Clowe et al. (2000) and by J01 the eastern weak lensing clump is X-ray dark. It is unclear why this mass density peak is not seen in X-rays. As J01 suggested, MS 1054–0321 could be in a pre-merger state given the clear separations of the two X-ray peaks. In this scenario the eastern weak lensing peak could still be forming and not be yet virialized, and it is thus underluminous in X-rays.

2.4. Point Source to the South

In order to examine the point source to the south, a circle of $0.33'$ was centered at $\alpha_{2000} = 10^h 56^m 58.8^s$, $\delta_{2000} = -03^{\circ} 38' 52''$. There are only a total of 454 ± 24 net counts in the source. Fitting to an absorbed power law gives a $N_H = (1.7 \pm 0.7) \times 10^{21}$ atoms cm^{-2} with a photon index $\Gamma = 1.9 \pm 0.2$, and a reduced χ^2 of 0.97 for 23 degrees of freedom. Both the column density (higher than the Galactic value) and the power law values are in very good agreement with the Chandra analysis by J01, who find a power law with a photon index $\Gamma = 1.7 \pm 0.3$, and a $N_H = 2.2_{-1.4}^{+1.8} \times 10^{21}$ atoms cm^{-2} . The observed flux in the 2–10 keV energy band for this source is $F_X = (3.0 \pm 1.0) \times 10^{-14}$ erg $\text{cm}^{-2} s^{-1}$. An X-ray spectrum is given in Fig. 6. The X-ray parameters are reported in Table 3. The optical image shows a quasi stellar object for which no optical spectroscopy was performed. We do not have an identification for this source. However its point-like appearance in the optical image plus the X-ray spectrum which has a photon index typical of Seyfert 1 active galactic nuclei suggest that the source could be an AGN.

3. Optical Data

Deep optical CCD images of MS 1054–0321 from the ground and from space have been acquired by several investigators in order to perform weak lensing studies and morphological analyses of the cluster galaxy population (Clowe et al. 2000; Hoekstra, Franx & Kuijken 2000; van Dokkum et al. 2000). van Dokkum et al. (1999) discover a high fraction of galaxy mergers in MS 1054–0321 which argues against formation of elliptical galaxies in a single “monolithic” collapse at high redshift but is in qualitative agreement with predictions of hierarchical models for structure formation. An impressive $4' \times 6'$ HST mosaic obtained with deep WFPC2 images in two colors is published in van Dokkum et al. (2000). The mosaic shows the filamentary appearance of MS 1054–0321: the cluster is easily identified as the horizontal and broad swath of red galaxies in the center of the frame. The cluster has also been observed several times at the Keck telescope to obtain spectroscopic redshifts for the member galaxies (Donahue et al. 1998; Tran et al. 1999; van Dokkum et al. 2000).

A larger number of spectroscopic redshifts mainly taken at the Keck telescope of both field galaxies and cluster members have been gathered by one of us (K-VT) and her collaborators. From a magnitude selected sample Tran et al. (in preparation) have spectroscopically confirmed cluster membership for 145 galaxies in a $7' \times 7'$ region centered on the cluster. From this large sample, they determine the cluster mean redshift and velocity dispersion to be $z=0.8308 \pm 0.0006$ and $\sigma_V = 1153 \pm 80$ km s^{-1} , with smaller uncertainties with respect to previous determinations by these same authors. MS 1054–0321 may well be the only $z=0.8$ cluster today with such a huge number of redshift determinations. The substructure evident in both X-ray and weak-lensing maps is also observed in the optical. The most significant optically identified subcluster lies $45''$ east of the BCG (Bright Cluster Galaxy) and, in comparison to the bulk of cluster members, is at lower redshift ($z=0.8281 \pm 0.0016$) and has a smaller velocity dispersion ($\sigma_V = 1061 \pm 168$ km s^{-1}). This clump is the only significant clump identified using the Dressler-Shectman test (Dressler & Shectman 1988). A direct comparison among the clumps in X-ray, weak lensing and optical data is not straightforward since the peaks do not coincide in the three wavebands. We have placed optical circles corresponding to the eastern and western X-ray clumps for comparison purposes. Redshifts and velocity dispersions have been recomputed for the galaxies in the two X-ray clumps. These data are presented in Table 4. The discrepancy in their mean redshifts and their large dispersions illustrates how unrelaxed MS 1054–0321 is and how much the distribution of the X-ray gas deviates from the optical distribution of galaxies.

4. Results and Discussion

The main result from the new XMM-Newton data is the lower measured value for the temperature of MS 1054–0321 with respect to previous determinations. The XMM-Newton temperature, $T=7.2_{-0.6}^{+0.7}$ keV, is definitely lower than the ASCA temperature $T=12.3_{-2.2}^{+3.1}$ keV (Donahue et al. 1998), and also somewhat lower, even taking into account the uncertainties, than the Chandra temperature, $T=10.4_{-1.5}^{+1.7}$ keV, reported by J01. It is however

fully consistent with the Chandra temperature, $T=7.8\pm 0.6$ keV, published by Vikhlinin et al. (2002) (see their Table 2), and with the Chandra temperature, $T=8.0\pm 0.5$ keV, published by Tozzi et al. (2003) (see their Table 3). The iron abundance inferred from the XMM-*Newton* observations is found to be in very good agreement with previous determinations by both J01 ($Z=0.38\pm 0.15 Z_{\odot}$) and by Tozzi et al. (2003) ($Z=0.35\pm 0.07 Z_{\odot}$) after their abundances are rescaled to the Grevesse & Sauval (1998) values while Vikhlinin et al. (2002) fix the abundance to $Z=0.3 Z_{\odot}$. MS 1054–0321 is in many aspects very similar to other distant X-ray selected clusters like RXJ 1717+67 at $z = 0.81$ (Gioia et al. 1999), or RXJ 0152.7–1357 at $z = 0.83$ (Della Ceca et al. 2000; Ebeling et al. 2000) which show elongated or double morphologies in optical, weak lensing and X-rays and which have moderate temperature values.

While it is possible that ASCA included other sources in its larger field of view, the lower X-ray temperature found for this cluster by this analysis, seems to be more accurate given the agreement of three out of four measurements (this paper; Vikhlinin et al., 2002; Tozzi et al., 2003). In order to verify the correctness of our XMM-*Newton* results we have analyzed the Chandra archival data of MS 1054–0321 and used all the information in the J01 paper to duplicate exactly their data reduction. There is a number of corrections to be made to the data. One of them, the ACISABS correction⁵, was not available at the time of the J01 analysis and was implemented later in the suggested steps for Chandra data reduction. This correction takes into account the quantum efficiency degradation at low energies, below 1 keV. The application of the ACISABS correction shifts the temperature towards lower values. There are several flares in the Chandra data, mostly visible only in the ACIS S3 back-illuminated chip, which contribute to raise the temperature. In the following analysis we use: a 1.5' extraction radius at the same cluster center as J01, the 0.8–7 keV energy range for the spectral fit, subtraction of point sources including the one to the south at the same position as J01, local background estimate, use of the Anders & Grevesse abundance values, counts binned in intervals so as to have at least 20 counts per bin, fit with a Raymond-Smith (Raymond & Smith 1977) thermal plasma model, N_H fixed to the Galactic value, temperature and abundance left free to vary. The two different parameters used are a lower exposure time of 67,478s (to cut out the time intervals affected by the flares) and application of the ACISABS correction. We obtain a value for the Chandra temperature $T=7.4^{+1.4}_{-0.9}$ keV, and an abundance $Z=0.20\pm 0.14 Z_{\odot}$, fully consistent with our XMM-*Newton* spectral result. If instead we release the two corrections (ACISABS, lower exposure time) then we obtain the same values as published by J01, namely $T=10.1^{+1.7}_{-1.5}$ keV and $Z=0.22\pm 0.16 Z_{\odot}$. Adopting all the corrections and the same parameters as in Vikhlinin et al. (2002) we obtain exactly their same value for the temperature $T=7.8\pm 1$ keV. Thus we are confident that our XMM-*Newton* data analysis is correct since the two different datasets, XMM-*Newton* and Chandra, yield exactly the same result.

We check now how MS 1054–0321 fits in the $L_X - T_X$ relation of galaxy clusters. Understanding the evolution of the $L_X - T_X$ relation is important not only to understand the physics behind the formation of galaxy clusters, but also because it provides a link between observations of clusters and derivation of cosmological parameters. The $L_X - T_X$ relation has been well studied at low redshift. There is no consensus yet on the evolution of the $L_X - T_X$ relation with redshift (see among others: Borgani et al. 2001; Holden et al. 2002; Novicki et al. 2002; Vikhlinin et al. 2002) probably due to the lack of large samples of galaxy clusters at cosmologically significant redshift. By comparing the bolometric luminosity of MS 1054–0321 with the best fit relationship $\log(L_{BOL,X}) = (2.88 \pm 0.15)\log(T/6\text{keV}) + (45.06 \pm 0.03)$ by Arnaud & Evrard (1999), or using similar observationally determined relationships, one would expect for MS 1054–0321 a temperature $T=8.2\pm 0.15$ keV which is well in agreement within the errors with the measured XMM-*Newton* temperature.

We check next the $\sigma_V - T_X$ relationship. We can estimate the velocity dispersion for MS 1054–0321 from the X-ray data and compare the result with the optical data. The velocity dispersion implied by the XMM-*Newton* temperature using the relation $T_X/\mu m_p \sigma^2$ with $\beta = 1$ (that is assuming energy equipartition between the galaxies and the gas) is $\sigma_V = 1047^{+50}_{-44}$ km s⁻¹, consistent with the observed optical velocity dispersion within the errors, implying that the velocity dispersion reflects the temperature of the gas. Girardi et al. (1996) have derived a best fit relation between the velocity dispersion and the X-ray temperature equal to $\text{Log}(\sigma) = (2.53 \pm 0.04) + (0.61 \pm 0.05)\log(T)$, with more than 30% reduced scatter with respect to previous work by taking into account distortions in the velocity fields, asphericity of the cluster or presence of substructures. Using the temperature $T=7.2$ keV of MS 1054–0321 in the above relation, the resulting velocity dispersion value, $\sigma_V = 1129^{+66}_{-57}$ km s⁻¹, is in very good agreement with the measured optical value, $\sigma_V = 1153 \pm 80$ km s⁻¹. The relation between temperature and velocity dispersion has been published by several authors. Last in order of time, this relation can be found in Lubin, Mulchaey & Postman (2003) where the authors have collected the information known today for all clusters at redshifts of $z \leq 1.27$ with a measured X-ray temperature. There is a big scatter in the $\sigma_V - T_X$ relation (see their figure 4) but the average relation is consistent with $\sigma \propto T^{1/2}$ up to these redshifts. We find that MS 1054–0321 follows closely this correlation.

We can also estimate the mass of MS 1054–0321 using the X-ray temperature value. With the assumptions that the mean density in the virialized region is ~ 200 times the critical density at the redshift of the cluster and that the cluster is isothermal (Evrard, Metzler & Navarro 1996; Donahue et al. 1998), we can use the scaling law method as illustrated

⁵ <http://www.astro.psu.edu/users/chartas/xcontdir/xcont.html>

Fig. 7. 21,600s I-band image of MS 1054–0321 taken at the 2.2m of the University of Hawai‘i. The smoothed overlaid X-ray contours are in units of 3, 5, 7, 10, 15, 20, 30, 35, 40, 43, 45 σ over the background. The image measures 2048×2048 pixels covering a field of $7'.5 \times 7'.5$ ($1.86h \times 1.86h$ Mpc at $z = 0.83$). Figure 7 can be seen in the pdf file of the paper at <http://www.ira.cnr.it/~gioia/PUB/publications.html>

in Arnaud & Evrard (1999). From the simulations of Evrard, Metzler & Navarro (1996) for the mass-temperature relation one can estimate the virial mass within a radius $r_{200}(T) = 1.85(T/10\text{keV})^{1/2}(1+z)^{-3/2} h^{-1}$ Mpc by using the equation $M_{vir} \approx (1.45 \times 10^{15} h^{-1} M_{\odot})(1+z)^{-3/2}(kT_X/10\text{keV})^{1.5}$. From the XMM-*Newton* temperature the virial mass is approximately $M_{vir} = (3.58_{-0.44}^{+0.53}) \times 10^{14} M_{\odot}$ within $r_{200} = 0.63 h^{-1}$ Mpc, where the uncertainties on the mass reflect the uncertainties on the temperature. This mass is lower than the one derived by J01 ($M \leq 0.76 h_{100}^{-1}$ Mpc = $6.2 \times 10^{14} h_{100}^{-1} M_{\odot}$) because they use a higher Chandra temperature which, given the relation between r_{200} and T , converts in a larger r_{200} (their $0.76 h_{100}^{-1}$ Mpc vs our $0.63 h_{100}^{-1}$ Mpc). The virial mass derived from the XMM-*Newton* temperature is definitely lower than the mass derived from weak lensing by Hoekstra, Franx & Kuijken (2000) of $1.2 \pm 0.2 \times 10^{15} h_{50}^{-1} M_{\odot}$ who used a different aperture radius of $1 h_{50}^{-1}$ Mpc. It is not possible with the present XMM-*Newton* data to assume an aperture radius of $1 h_{50}^{-1}$ Mpc ($1.75'$ using the Hoekstra et al. cosmology) since we are running into the gaps between the chips for the pn detector.

Given the XMM-*Newton* results, MS 1054–0321 appears to be a more “normal” cluster with high, but not extreme X-ray luminosity or temperature values. Its temperature seems to be commensurate with the predictions from its X-ray luminosity from the $L_X - T_X$ relation of local clusters published in the literature. The optically measured velocity dispersion is consistent with the velocity dispersion expected from the $\sigma_V - T_X$ relationship. Given the clear evidence for substructure in the cluster morphology, indicative of a still unrelaxed cluster, it is surprising that the global properties of MS 1054–0321 fit so well in any local cluster correlation.

5. Summary

We have presented new observations for the $z=0.83$ galaxy cluster MS 1054–0321 performed with the instruments on board the XMM-*Newton* satellite. The main result of this paper is the lower value indicated by the XMM-*Newton* observations for the overall cluster X-ray temperature with respect to some of the previous analyses. Excluding the contribution of the southern point source the temperature of the cluster is $T=7.2_{-0.6}^{+0.7}$ keV. If one allows the column density to be a free parameter then the best fit temperature is $T=8.6_{-1.1}^{+1.2}$ keV, and the best fit column density becomes $N_H = 1.33_{-0.14}^{+0.15} \times 10^{20}$ atoms cm^{-2} . The iron line is well detected with a value for the abundance of $Z=0.33_{-0.18}^{+0.19} Z_{\odot}$. The point source to the south is fitted by an absorbed power law with $N_H = (1.7 \pm 0.7) \times 10^{21}$ atoms cm^{-2} and a photon index $\Gamma=1.9 \pm 0.2$. The XMM-*Newton* data confirm the substructure in the cluster X-ray morphology already seen by previous experiments. The two main clumps have very different temperatures. The eastern clump is hotter ($T=8.1_{-1.2}^{+1.3}$ keV) compared to the western clump ($T=5.6_{-0.6}^{+0.8}$ keV), as also found by J01. MS 1054–0321 has an X-ray luminosity in the 2–10 keV energy band of $L_X = (3.81 \pm 0.19) \times 10^{44} h^{-2}$ erg s^{-1} and a bolometric luminosity of $L_{BOL} = (8.05 \pm 0.40) \times 10^{44} h^{-2}$ erg s^{-1} . The velocity dispersion derived from the X-ray temperature for the whole cluster is in good agreement with the most recent determination of the observed velocity dispersion derived from a much enlarged database of 145 cluster member redshifts. MS 1054–0321 fits well in the $\sigma \propto T^{1/2}$ correlation available in the literature and derived from information collected for all clusters at redshifts of $z \leq 1.27$ known today and with a measured X-ray temperature.

We have discussed in detail the discrepancy between the XMM-*Newton* and Chandra derived temperatures and found that the origin of this discrepancy is mainly due to corrections to be implemented in the Chandra data to obtain a much cleaner dataset. An analysis of the Chandra archival data taking into account all the possible corrections yields a temperature $T=7.4_{-0.9}^{+1.4}$ keV, in excellent agreement with the XMM-*Newton* determined temperature value. Given these results MS 1054–0321 is no longer amongst the hottest clusters known but it is more similar to other X-ray selected clusters in the same redshift range with moderate temperatures and elongated or double morphologies seen in different waveband domains.

Acknowledgements. We are grateful to G. Illingworth and M. Franx for access to the MS 1054–0321 Keck spectroscopic database, and to the referee, M. Donahue, who made many constructive criticisms which improved this paper.

References

- Anders, E. & Grevesse, N. 1989, *Geochim. Cosmochim. Acta*, 53, 197
 Arnaud, M. & Evrard A. E. 1999, *MNRAS*, 305, 631
 Best, P.N., van Dokkum, P.G., Franx, M. & Röttgering, H.J.A. 2002, *MNRAS*, 330, 17

- Bevington, P.R. & Robinson, D.K. Data Reduction and Error Analysis for the Physical Sciences 1992, New York: McGraw-Hill, publishers
- Borgani, S. et al. 2001, ApJ, 561, 13
- Clowe, D., Luppino, G.A., Kaiser, N. & Gioia, I.M. 2000, ApJ, 539, 540
- Della Ceca, R., Scaramella, R., Gioia, I.M., Rosati, P., Fiore, F. & Squires, G. 2000, A&A, 353, 498
- Dickey, J.N. & Lockman, F.J. 1990, ARA&A, 28, 215
- Donahue, M., Voit, G.M., Gioia, I., Luppino, G., Hughes, J. & Stocke, J. 1998, ApJ, 502, 550
- Dressler, A. & Shectman, S. A. 1988, AJ, 95, 284
- Ebeling, H., Jones, L.R., Perlman, E., Scharf, C., Horner, D., Wegner, G., Malkan, M., Fairley, B. W. & Mullis, C. R. 2000, ApJ, 534, 133
- Evrard, A.E., Metzler, C.A. & Navarro, J.F. 1996, ApJ, 469, 494
- Gastaldello, F. & Molendi, S. 2002, ApJ, 572, 160
- Gioia, I.M., Maccacaro, T., Schild, R.E., Wolter, A., Stocke, J.T., Morris, S.L. & Henry, J.P. 1990, ApJS, 72, 567
- Gioia, I.M. & Luppino, G.A. 1994, ApJS, 94, 583
- Gioia, I.M., Henry, J.P., Mullis, C.R., Ebeling, H. & Wolter, A. 1999, AJ, 117, 2608
- Girardi, M., Fadda, D., Giuricin, G., Mardirossian, F. and Mezzetti, M. 1996, ApJ, 457, 61
- Grevesse, N. & Sauval, A.J. 1998, Space Sci. Rev., 85, 161
- Hoekstra, H., Franx, M. & Kuijken, K. 2000 ApJ, 532, 88
- Holden, B.P., Stanford, S.A., Squires, G.K., Rosati, P., Tozzi, P., Eisenhardt, P. & Spinrad, H. 2002, AJ, 124, 33
- Jeltema, T.E., Canizares, C.R., Bautz, M.W., Malm, M.R., Donahue, M., & Garmire, G.P. 2001, ApJ, 562, 124 (J01)
- Johnson, O., Best, P.N. & Almaini, O. 2003, MNRAS, 343, 924
- Joy, M., LaRoque, S., Grego, L., Carlstrom, J.E., Dawson, K., Ebeling, H., Holsapfel, W.L., Nagai, D. Reese, E.D. 2001, ApJ, 551 L1
- Lubin, L.M., Mulchaey, J.S. & Postman, M. 2004, ApJ, 601, L9
- Luppino, G.A. & Kaiser, N. 1997, ApJ, 475, 20
- Mewe, R., Gronenschild, E.H.B.M. & van den Oord, G.H.J. 1985, A&AS, 62, 197
- Neumann, D.M. & Arnaud, M. 2000, ApJ, 542, 35
- Novicki, M. C., Sornig, M. & Henry, J.P. 2002, AJ, 124, 2413
- Raymond, J.C. & Smith, B.W. 1977, ApJS, 35, 419
- Strüder, L. et al. 2001, A&A, 365, L18
- Stocke, J.T., Morris, S.L, Gioia, I.M., Maccacaro, T., Schild, R.E., Wolter, A., Fleming, T.A. & Henry, J.P 1991, ApJS, 76, 813
- Tozzi, P., Rosati, P., Ettori, S., Borgani, S., Mainieri, V. & Norman, C. 2003, ApJ, 593, 705
- Tran, K-V. H., Kelson, D.D., van Dokkum, P.G., Franx, M., Illingworth, G.D. & Magee, D. 1999, ApJ, 522, 39
- Turner, M.J.L. et al. 2001, A&A, 365, L27
- van Dokkum, P.G., Franx, M., Fabricant, D., Kelson, D.D. & Illingworth, G.D. 1999, ApJ, 520, L95
- van Dokkum, P.G., Franx, M., Fabricant, D., Illingworth, G.D. & Kelson, D.D. 2000, ApJ, 541, 95
- Vikhlinin, A., VanSpeybroeck, L., Markevitch, M., Forman, W. R. & Grego, L. 2002, ApJ, 578, L107

Table 1. X-RAY PROPERTIES OF MS 1054–0321

RA (J2000) h m s	DEC (J2000) ° ' "	Instr	R '	Net Cts 2–10 keV	T keV	Z Z_{\odot}	N_H $\times 10^{20}$ at/cm ²	Region
10 56 58.7	-03 37 45				$7.2^{+0.7}_{-0.6}$	$0.33^{+0.19}_{-0.18}$	frozen ^a	whole cluster
					$8.6^{+1.2}_{-1.1}$	$0.22^{+0.15}_{-0.14}$	$1.33^{+0.15}_{-0.14}$	whole cluster
		MOS1	1.5	2198±52				
		MOS2	1.5	2392±54				
		pn	1.5	4486±75				
10 57 00.3	-03 37 29				$8.1^{+1.3}_{-1.2}$	$0.12^{+0.35}_{-0.12}$	frozen ^a	Component 1
		MOS1	0.47	583±25				
		MOS2	0.47	604±25				
		pn	0.47	1200±36				
10 56 56.6	-03 37 36				$5.6^{+0.8}_{-0.6}$	$0.51^{+0.36}_{-0.32}$	frozen ^a	Component 2
		MOS1	0.47	524±24				
		MOS2	0.47	575±25				
		pn	0.47	1146±36				

^a N_H fixed at the Galactic value of 3.6×10^{20} atoms cm⁻²

Table 2. FLUXES AND LUMINOSITIES FOR THE CLUSTER COMPONENTS

RA (J2000) h m s	DEC (J2000) ° ' "	F_X (2–10 keV) $\times 10^{-13}$ erg cm ⁻² s ⁻¹	L_X (2–10 keV) $\times 10^{44}$ erg s ⁻¹	L_{BOL} $\times 10^{44}$ erg s ⁻¹	Region
10 56 58.7	-03 37 45	3.40±0.17	3.81±0.19	8.05±0.40	whole cluster
10 57 00.3	-03 37 29	0.97±0.07	1.05±0.07	2.23±0.15	eastern Component 1
10 56 56.6	-03 37 36	0.69±0.06	0.87±0.07	1.82±0.15	western Component 2

Table 3. X-RAY PROPERTIES OF THE POINT SOURCE TO THE SOUTH

RA (J2000) h m s	DEC (J2000) ° ' "	Instr	R '	Net Cts	N_H $\times 10^{21}$ at/cm ²	Γ	Flux (2–10 keV) $\times 10^{-14}$ erg cm ⁻² s ⁻¹
10 56 58.8	-03 38 52				1.7 ± 0.7	1.9 ± 0.2	3.0 ± 1
		MOS1	0.33	101±11			
		MOS2	0.33	89±11			
		pn	0.33	264±18			

Table 4. OPTICAL AND X-RAY PROPERTIES OF THE TWO CLUSTER COMPONENTS

RA (J2000) h m s	DEC (J2000) ° ' "	R '	N_{gals}	$\langle z \rangle$	σ_V km s ⁻¹	T_X keV	L_{BOL} 10 ⁴⁴ erg s ⁻¹
10 57 00.3	-03 37 28.8	0.47	17	0.8297±0.0020	1225±250	8.1	2.23
10 56 56.6	-03 37 36.3	0.47	11	0.8342±0.0022	1353±315	5.6	1.82